A Simple Passive Attitude Stabilizer for Palm-size Aerial Vehicles

Motoyasu Tanaka, *Member, IEEE,* Ying Jen Chen, *Member, IEEE,* Kazuo Tanaka, *Fellow, IEEE,* and Hua O. Wang, *Senior Member, IEEE*

***Abstract*— This paper presents a simple passive attitude stabilizer (PAS) for vision-based stabilization of palm-size aerial vehicles. First, a mathematical dynamic model of a palm-size aerial vehicle with the proposed PAS is constructed. Stability analysis for the dynamics is carried out in terms of Lyapunov stability theory. The analysis results show that the proposed stabilizer guarantees passive stabilizing behavior, i.e., passive attitude recovering, of the aerial vehicle for small perturbations from a stability theory point of view. Experimental results demonstrate the utility of the proposed PAS for the aerial vehicle.**

***Index Terms*— Lyapunov stability theory, palm-size aerial vehicle, passive attitude stabilizer.**

I. Introduction

In recent years, small-scale aerial vehicles (like palm-size indoor helicopters), e.g., [1]-[4], have received great attention in the research literature of unmanned aerial vehicles (UAVs) [5] -[7] and micro air vehicles (MAVs) [8]-[9]. Despite recent advances, autonomous control of MAVs remains a challenging problem. Since MAVs cannot fly for a long time and are seriously influenced by wind conditions, MAVs are suitable for indoor use. However, GPS is not available for measuring their position in indoor environments. In addition, MAVs have limited payload. Stabilization for indoor palm-size helicopters has been reported in [1]-[4]. Due to the payload limit as well as the absence of GPS signals, these studies employ *external* sensors like CCD camera-type vision sensors to stabilize the indoor helicopters. Instead of constructing control systems using *external* sensors, in this paper, we construct a control system for a palm-size helicopter using only an on-board wireless vision sensor. Specifically, we develop a simple and lightweight PAS to assist stable flight of the palm-size helicopter with only a wireless vision sensor. The use of a wireless vision (internal) sensor is suitable for our eventual research objective of gathering visual information in narrow indoor space. Further discussion of this aspect is presented in Section V.

There exist a number of stabilizers, e.g., bell-hiller bar [10], tilting rotator of picoflyer [11], etc., for helicopters. Since the main blade cyclic in bell-hiller control systems is controlled partly by flybar tilt and partly by direct cyclic control from a swash plate, it is not lightweight. Therefore, due to the payload limitation (60 [g] in our aerial vehicle), it is not available for palm-size aerial vehicles. Though the tilting rotor of the picoflyer is not heavyweight, it is basically the same structure as the well-known co-axial counter rotating type helicopter. Only the anti-torque is cancelled by co-axial counter rotating blade. However it has no self-recovering stabilizing properties in the attitude (the roll and pitch angles). Thus, in [10], [11], the effect of stabilizers was not discussed.

This paper presents a simple, lightweight and novel PAS, that realizes passively stabilization of the attitude (the roll and pitch angles) without (active) feedback control, for '*vision-based*' stabilization of indoor '*palm-size*' aerial vehicles. With the aforementioned payload limitation, inertial measurement units (IMUs) are not suited to use as position and attitude sensors due to their heavyweight. Moreover GPS is not available for indoor environments. We solve these problems by employing a single and lightweight CCD camera-type vision sensor for position and attitude measurement. Vision sensors are generally low precision in comparison with the IMU-based measurement. Therefore, it is difficult to stabilize aerial vehicles only using a single vision sensor in real world experiments. The passive stabilizer developed in this paper renders stable flight in real world environments. The passive stabilizer is analyzed in terms of Lyapunov stability theory. Experimental results demonstrate the utility and effectiveness of the stabilizer.

II. Passive Attitude Stabilizer

Fig. 1 shows the R/C palm-size helicopter and the experimental system. The sampling rate is 30 [Hz]. The palm-size helicopter is a co-axial counter rotating type helicopter. The

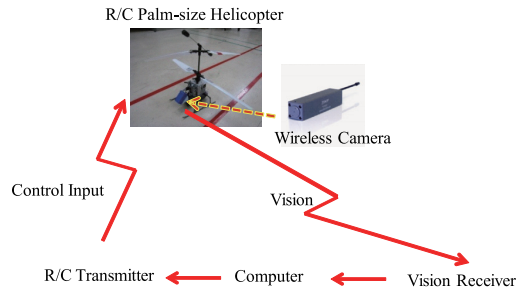

Fig. 1. R/C palm-size helicopter and experimental system.

Manuscript received Jan. 1, 2013; revised November XX, 20XX. This work was supported in part by a Grant-in-Aid for Scientific Research (C) 25420215 from the Ministry of Education, Science and Culture of Japan.

M. Tanaka, Y. J. Chen and K. Tanaka are with the Department of Mechanical Engineering and Intelligent Systems, The University of Electro-Communications, Chofu, Tokyo 182-8585 Japan (email:mtanaka@uec.ac.jp; chen@rc.mce.uec.ac.jp; ktanaka@mce.uec.ac.jp).

H. O. Wang is with the Department of Mechanical Engineering, Boston University, Boston, MA 02215 USA (email: wangh@bu.edu).

weight of the small-light wireless camera is 55 [g] and is not over the payload limitation (60 [g]). The position and attitude of the helicopter are calculated by an open-source software, PTAM[12], based on vision obtained from the wireless camera. The PTAM is a method of estimating camera pose (only by a single camera) in an unknown scene.

A key feature of realizing the passive stabilization is to utilize the moment of anti-gravity. To generate the moment, we use a Helium gasbag that is lighter than the air. Fig. 2 shows the palm-size helicopter attaching the PAS. An important point is that the flight concept of our palm-size helicopter attaching the stabilizer is completely different from that of lighter-than-air (blimp) platforms utilizing lift forces generated from Helium gas [13], [14]. The lighter-than-air (blimp) platforms generate 100% lift forces from Helium gas. On the other hand, the passive stabilization can be realized with a gasbag generating only 9.79% $(= 23[g]/235[g] \times 100)$ lift force of the overall weight 235 [g].

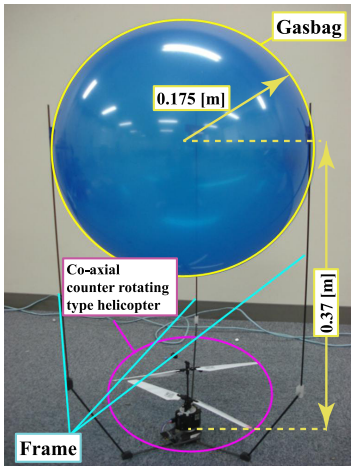

Fig. 2. Palm-size helicopter attaching passive attitude stabilizer.

III. Passive stability analysis

The dynamics of the helicopter in the body-fixed frame can be described as (1)-(6) [15].

$$m(\dot{u}(t) + q(t)w(t) - r(t)v(t)) = F_X(t), \quad (1)$$
$$m(\dot{v}(t) + r(t)u(t) - p(t)w(t)) = F_Y(t), \quad (2)$$
$$m(\dot{w}(t) + p(t)v(t) - q(t)u(t)) = F_Z(t), \quad (3)$$
$$I_X\dot{p}(t) + (I_Z - I_Y)q(t)r(t) = M_X(t), \quad (4)$$
$$I_Y\dot{q}(t) + (I_X - I_Z)r(t)p(t) = M_Y(t), \quad (5)$$
$$I_Z\dot{r}(t) + (I_Y - I_X)p(t)q(t) = M_Z(t). \quad (6)$$

The dynamics consist of the force equations (1)-(3) and the moment equations (4)-(6). Table I shows the definition of variables and parameters used in the dynamic model in the body-fixed frame, where X, Y and Z axes denote longitudinal/roll, lateral/pitch and vertical/yaw axes, respectively. Table II shows a list of other variables and parameters excepting those shown in Table I. The body angular velocities can be represented in terms of Euler angles and Euler rates.

$$p(t) = \dot{\phi}(t) - \dot{\psi}(t)S_\theta(t), \quad (7)$$
$$q(t) = \dot{\theta}(t)C_\phi(t) + \dot{\psi}(t)C_\theta(t)S_\phi(t), \quad (8)$$
$$r(t) = \dot{\psi}(t)C_\theta(t)C_\phi(t) - \dot{\theta}(t)S_\phi(t), \quad (9)$$

where $\phi(t)$, $\theta(t)$, $\psi(t)$ denote the Euler angles. $S_\phi(t)$, $C_\phi(t)$ and $T_\theta(t)$ denotes $\sin\phi(t)$, $\cos\phi(t)$ and $\tan\theta(t)$, respectively. The Euler rates can be represented in terms of the Euler angles and the body angular velocities.

$$\dot{\phi}(t) = p(t) + q(t)S_\phi(t)T_\theta(t) + r(t)C_\phi(t)T_\theta(t), \quad (10)$$
$$\dot{\theta}(t) = q(t)C_\phi(t) - r(t)S_\phi(t), \quad (11)$$
$$\dot{\psi}(t) = q(t)S_\phi(t)\sec\theta(t) + r(t)C_\phi(t)\sec\theta(t). \quad (12)$$

Note that the X, Y and Z axes in Table I are defined in the body-fixed frame. The definition is the same as those in standard literature [15]. The x, y and z axes (in the inertial frame) in Sections III, IV and V are appropriately defined in the indoor experimental field. Velocities in the inertial frame are obtained in terms of the Euler angles and the body velocity components.

$$\begin{bmatrix} \frac{dx(t)}{dt} \\ \frac{dy(t)}{dt} \\ \frac{dz(t)}{dt} \end{bmatrix} = \boldsymbol{R}(\phi(t), \theta(t), \psi(t)) \begin{bmatrix} u(t) \\ v(t) \\ w(t) \end{bmatrix},$$

where

$$\boldsymbol{R}(\phi(t), \theta(t), \psi(t)) = \begin{bmatrix} C_\theta C_\psi & S_\phi S_\theta C_\psi - C_\phi S_\psi & C_\phi S_\theta C_\psi + S_\phi S_\psi \\ C_\theta S_\psi & S_\phi S_\theta S_\psi - C_\phi C_\psi & C_\phi S_\theta S_\psi - S_\phi C_\psi \\ -S_\theta & S_\phi C_\theta & C_\phi C_\theta \end{bmatrix}. \quad (13)$$

TABLE I
Definition of variables and parameters in body-fixed frame.

u, v, w	velocity (X-axis, Y-axis, Z-axis)
p, q, r	angular velocity (X-axis, Y-axis, Z-axis)
m	mass (m=0.235kg)
I_X, I_Y, I_Z	moments of inertia with respect to X, Y and Z axes ($I_X = I_Y = 3.4 \times 10^{-3}, I_Z = 1.8 \times 10^{-3} kg \cdot m^2$)
F_X, F_Y, F_Z	translational forces to X, Y and Z axes
M_X, M_Y, M_Z	rotational forces around X, Y and Z axes

TABLE II
Definition of other variables and parameters.

ϕ, θ, ψ	Euler angles
$\dot{\phi}$, $\dot{\theta}$, $\dot{\psi}$	Euler rates
h	distance between center of gasbag and center of gravity
r_a	radius of gasbag
g	acceleration of gravity (9.80665 kg $\cdot m/s^2$)
ρ_a, ρ_h	densities of air (1.205 kg/m^3) and Helium (0.1785 kg/m^3)
C_D	cross-section drag coefficient of sphere (gasbag) (C_D=0.5)
μ	coefficient of viscosity of air (μ =1.82 $\cdot 10^{-5}$ kg $\cdot s/m^2$)

We start to consider dynamics of motion of the palm-size helicopter with the PAS for small perturbations (with respect to the roll and pitch angles). Therefore, we focus on the roll and pitch angles dynamics, i.e., (4) and (5). We assume that a small perturbation with respect to the roll and pitch angles is given

at any hovering positions. Hence, $\phi(t)$ and $\theta(t)$ caused by the small perturbation are small and note that $p(t) \simeq \dot{\phi}(t)$ and $q(t) \simeq \dot{\theta}(t)$. In this case, $M_X(t)$ and $M_Y(t)$ relate to the lift force L (generated by the gasbag), the inertial drag force, and viscous drag force of the gasbag. Due to symmetric structure of the co-axial counter rotating type helicopter, note that $I_X = I_Y$. Then, the roll and pitch angles dynamics including the gasbag dynamics can be obtained as

$$\begin{aligned} &I\dot{p}(t) + (I_Z - I)q(t)r(t) \\ &= -h^2 c_v \dot{\phi}(t) - h^3 c_i |\dot{\phi}(t)|\dot{\phi}(t) - LhS_\phi(t), \end{aligned} \tag{14}$$

$$\begin{aligned} &I\dot{q}(t) + (I - I_Z)r(t)p(t) \\ &= -h^2 c_v \dot{\theta}(t) - h^3 c_i |\dot{\theta}(t)|\dot{\theta}(t) - LhS_\theta(t), \end{aligned} \tag{15}$$

where $c_i = \frac{1}{2}\rho_a C_D(\pi r_a^2)$, $c_v = 6\pi\mu r_a$, $I = I_X = I_Y$. L ($L = \frac{4}{3}\pi r_a^3(\rho_a - \rho_h)g$) denotes the lift force of the gasbag. The first and second terms in the right sides of (14) and (15) denote the rotational forces generated by the viscous and inertial drag forces of the gasbag, respectively. The third terms denote the rotational force generated by the lift force L of the gasbag. Since $\sin\phi(t)$ can be approximated with $\phi(t)$ from the above assumptions, the roll and pitch dynamics of the palm-size helicopter with the PAS can be described as follows.

$$\boldsymbol{M}_p\ddot{\boldsymbol{x}}(t) + \boldsymbol{K}_p(\dot{\boldsymbol{x}}(t), r(t))\dot{\boldsymbol{x}}(t) + \boldsymbol{G}_p\boldsymbol{x}(t) = \boldsymbol{0}, \tag{16}$$

where $\boldsymbol{x}(t) = [\phi(t)\ \ \theta(t)]^T$, $\boldsymbol{M}_p = diag[I \quad I]$, $\boldsymbol{G}_p = diag[Lh \quad Lh]$,

$$\boldsymbol{K}_p(\dot{\boldsymbol{x}}(t), r(t)) = \begin{bmatrix} h^2 c_v + h^3 c_i|\dot{\phi}(t)| & r(t)(I_Z - I) \\ -r(t)(I_Z - I) & h^2 c_v + h^3 c_i|\dot{\theta}(t)| \end{bmatrix}.$$

Now let us consider a candidate of the following Lyapunov function $V_1(\boldsymbol{x}(t), \dot{\boldsymbol{x}}(t))$.

$$V_1(\boldsymbol{x}(t), \dot{\boldsymbol{x}}(t)) = \frac{1}{2}\dot{\boldsymbol{x}}^T(t)\boldsymbol{M}_p\dot{\boldsymbol{x}}(t) + \frac{1}{2}\boldsymbol{x}^T(t)\boldsymbol{G}_p\boldsymbol{x}(t) \tag{17}$$

Note that $V_1(\boldsymbol{x}(t), \dot{\boldsymbol{x}}(t)) = 0$ at $\boldsymbol{x}(t) = \boldsymbol{0}$ and $\dot{\boldsymbol{x}}(t) = \boldsymbol{0}$, and $V_1(\boldsymbol{x}(t), \dot{\boldsymbol{x}}(t)) > 0$ at $\boldsymbol{x}(t) \neq \boldsymbol{0}$ and $\dot{\boldsymbol{x}}(t) \neq \boldsymbol{0}$ since $\boldsymbol{M}_p > \boldsymbol{0}$ and $\boldsymbol{G}_p > \boldsymbol{0}$. In addition, $V_1(\boldsymbol{x}(t), \dot{\boldsymbol{x}}(t))$ is radially unbounded. By taking time derivative along the trajectory of (16), $\dot{V}_1(\boldsymbol{x}(t), \dot{\boldsymbol{x}}(t))$ can be calculated as

$$\begin{aligned} &\dot{V}_1(\boldsymbol{x}(t), \dot{\boldsymbol{x}}(t)) = \frac{1}{2}\ddot{\boldsymbol{x}}^T(t)\boldsymbol{M}_p\dot{\boldsymbol{x}}(t) + \frac{1}{2}\dot{\boldsymbol{x}}^T(t)\boldsymbol{M}_p\ddot{\boldsymbol{x}}(t) \\ &+\frac{1}{2}\dot{\boldsymbol{x}}^T(t)\boldsymbol{G}_p\boldsymbol{x}(t) + \frac{1}{2}\boldsymbol{x}^T(t)\boldsymbol{G}_p\dot{\boldsymbol{x}}(t) \\ &= \frac{1}{2}(-\boldsymbol{K}_p(\dot{\boldsymbol{x}}(t), r(t))\dot{\boldsymbol{x}}(t) - \boldsymbol{G}_p\boldsymbol{x}(t))^T\dot{\boldsymbol{x}}(t) \\ &+\frac{1}{2}\dot{\boldsymbol{x}}^T(t)(-\boldsymbol{K}_p(\dot{\boldsymbol{x}}(t), r(t))\dot{\boldsymbol{x}}(t) - \boldsymbol{G}_p\boldsymbol{x}(t)) \\ &+\frac{1}{2}\dot{\boldsymbol{x}}^T(t)\boldsymbol{G}_p\boldsymbol{x}(t) + \frac{1}{2}\boldsymbol{x}^T(t)\boldsymbol{G}_p\dot{\boldsymbol{x}}(t) \\ &= -\dot{\boldsymbol{x}}^T(t)\boldsymbol{K}_p(\dot{\boldsymbol{x}}(t), r(t))\dot{\boldsymbol{x}}(t) \\ &= -(h^2 c_v + h^3 c_i|\dot{\phi}(t)|)\dot{\phi}^2(t) \\ &-(h^2 c_v + h^3 c_i|\dot{\theta}(t)|)\dot{\theta}^2(t). \end{aligned} \tag{18}$$

It should be noted that $V_1(\boldsymbol{x}(t), \dot{\boldsymbol{x}}(t))$ is a continuously differentiable, radially unbounded and positive definite function. $\dot{V}_1(\boldsymbol{x}(t), \dot{\boldsymbol{x}}(t))$ is always non-positive for any $\dot{\boldsymbol{x}}(t)$ since h, c_v and c_i are positive values. Note that

$$\begin{aligned} &-\dot{\boldsymbol{x}}^T(t)\boldsymbol{K}_p(\dot{\boldsymbol{x}}(t), r(t))\dot{\boldsymbol{x}}(t) \\ &\qquad = -\dot{\boldsymbol{x}}^T(t)diag(\boldsymbol{K}_p(\dot{\boldsymbol{x}}(t), r(t)))\boldsymbol{I}\dot{\boldsymbol{x}}(t). \end{aligned} \tag{19}$$

Let $S_1 = \{(\boldsymbol{x}(t), \dot{\boldsymbol{x}}(t)) \mid \dot{V}_1(\boldsymbol{x}(t), \dot{\boldsymbol{x}}(t)) = 0\}$. Then, it is clear that no solution can stay identically in S_1, other than the trivial solution $\boldsymbol{x}(t) = \boldsymbol{0}$ and $\dot{\boldsymbol{x}}(t) = \boldsymbol{0}$. Hence, from Krasovskii-LaSalle's principle, the origin of (16) is globally asymptotically stable [16]. Thus, the passive stability, $\phi(t) \to 0$ and $\theta(t) \to 0$, can be realized by using the proposed passive stabilizer. Section V will show that the PAS works well although the stabilizer is simple.

The moments of inertia play an important role. In fact, the second term in the Lyapunov function candidate (17) is constructed using the moment of inertia generated by the gasbag lift force. Taking the time derivative of (17) along the system trajectory, $\dot{V}_1(\boldsymbol{x}(t), \dot{\boldsymbol{x}}(t))$ is guaranteed to become negative excepting $\boldsymbol{x}(t) = 0$. Eq. (18) shows that $\dot{V}_1(\boldsymbol{x}(t), \dot{\boldsymbol{x}}(t))$ is represented using the moments of inertia generated from the viscous and inertial forces of the gasbag. Thus, we can see that the passive stability is guaranteed by the moments generated from the gasbag. In this paper, we design the parameters (h and r_a) of the stabilizer as follows: $r_a = 0.175$ and $h = 0.37$. Clearly, the passive stabilizer with any $h > 0$ and $r_a > 0$ guarantees passive stabilization for the roll and pitch angles dynamics. In addition, larger h and r_a realize faster convergence. Thus if larger h and r_a are selected, the performance of the passive stabilization becomes stronger. However it causes an enlargement of the aerial vehicle size. The gasbag with $r_a = 0.175$ generates about 23 [g] lift force. The whole body weight including the passive stabilizer is about 235 [g]. As mentioned before, the passive stabilization can be realized with a gasbag generating only 9.79% lift force of the overall weight, although other lighter-than-air (blimp) platforms generate 100% lift forces from Helium gas. If the gasbag is needed to have the 100% lift force for own weight, its volume becomes approximately 10 times larger than the volume of the current gasbag.

IV. Flight Control System Analysis

In Section IV, we analyze the flight control system that consists of the passive attitude (the roll and pitch angles) stabilizer and an active feedback controller (the yaw angle and position). The passive attitude stabilizer can be expected to weaken the strong coupling between the attitude and position. This fact means that it becomes easier to stabilize the yaw angle and position since the stabilizer achieves the passive stabilization of the roll and pitch angles. The fact will be found in experimental results later. Thus, if the palm-size helicopter has the stabilizer, it is enough to design a controller that stabilizes the yaw angle and the x, y, z positions. The remaining dynamics excepting the roll and pitch dynamics are described as (1)-(3) and (6). Since $I = I_Y = I_X$, the equations of motion can be described as follows. The matrix representation of (1)-(3) and (6) is rewritten as

$$\boldsymbol{M}_m\dot{\boldsymbol{\zeta}}(t) + \boldsymbol{K}_m(p(t), q(t), r(t))\boldsymbol{\zeta}(t) = \boldsymbol{u}(t), \tag{20}$$

where $\boldsymbol{\zeta}(t) = [u(t)\ v(t)\ w(t)\ r(t)]^T$, $\boldsymbol{u}(t) = [F_x(t)\ F_y(t)\ F_z(t)\ M_z(t)]^T$, $\boldsymbol{M}_m = diag\,[m\ m\ m\ m\ I_Z]$,

$$\boldsymbol{K}_m(p(t),q(t),r(t)) = \begin{bmatrix} 0 & -r(t) & q(t) & 0 \\ r(t) & 0 & -p(t) & 0 \\ -q(t) & p(t) & 0 & 0 \\ 0 & 0 & 0 & 0 \end{bmatrix}.$$

A simple feedback controller (the yaw angle and position) is designed to realize stable flight to desired waypoints.

$$\boldsymbol{u}(t) = -\boldsymbol{F}_1\boldsymbol{\zeta}(t) - \boldsymbol{T}^T(\psi(t))\boldsymbol{F}_2\boldsymbol{e}(t), \tag{21}$$

where $\boldsymbol{F}_1 > \boldsymbol{0}$, $\boldsymbol{F}_2 > \boldsymbol{0}$,

$$\boldsymbol{T}(\psi(t)) = \begin{bmatrix} \boldsymbol{R}(0,0,\psi(t)) & \boldsymbol{0}_{3\times 1} \\ \boldsymbol{0}_{1\times 3} & 1 \end{bmatrix}, \tag{22}$$

and $\boldsymbol{e}(t) = [e_x(t)\ e_y(t)\ e_z(t)\ e_\psi(t)]^T$, $e_x(t) = x(t) - r_x$, $e_y(t) = y(t) - r_y$, $e_z(t) = z(t) - r_z$ and $e_\psi(t) = \psi(t) - r_\psi$. r_x, r_y, r_z and r_ψ denote the constant target vaules of x, y, z and ψ, respectively. Note that $\dot{\psi}(t) \simeq r(t)$ from (11) and (12), and recall $q(t) \simeq \dot{\theta}(t)$ from the discussions in Section III. Therefore, we have the following relation between $\dot{\boldsymbol{e}}(t)$ and $\boldsymbol{\zeta}(t)$, $\dot{\boldsymbol{e}}(t) = \boldsymbol{T}(\psi(t))\boldsymbol{\zeta}(t)$. We can obtain the original control inputs (to the real helicopter, i.e., throttle, elevator, ailerons and rudder) from $F_X(t)$, $F_Y(t)$, $F_Z(t)$ and $M_z(t)$. By substituting (21) into (20), we have the dynamics of the feedback system.

$$\begin{aligned} \boldsymbol{M}_m\dot{\boldsymbol{\zeta}}(t) + (\boldsymbol{K}_m(p(t),q(t),r(t)) + \boldsymbol{F}_1)\boldsymbol{\zeta}(t) \\ + \boldsymbol{T}^T(\psi(t))\boldsymbol{F}_2\boldsymbol{e}(t) = \boldsymbol{0}. \end{aligned} \tag{23}$$

Now let us consider a candidate of the following Lyapunov function $V_2(\boldsymbol{e}(t),\boldsymbol{\zeta}(t))$.

$$V_2(\boldsymbol{e}(t),\boldsymbol{\zeta}(t)) = \frac{1}{2}\boldsymbol{\zeta}^T(t)\boldsymbol{M}_m\boldsymbol{\zeta}(t) + \frac{1}{2}\boldsymbol{e}^T(t)\boldsymbol{F}_2\boldsymbol{e}(t) \tag{24}$$

Note that $V_2(\boldsymbol{e}(t),\boldsymbol{\zeta}(t)) = 0$ at $\boldsymbol{e}(t) = \boldsymbol{0}$ and $\boldsymbol{\zeta}(t) = \boldsymbol{0}$, and $V_2(\boldsymbol{e}(t),\boldsymbol{\zeta}(t)) > 0$ at $\boldsymbol{e}(t) \neq \boldsymbol{0}$ and $\boldsymbol{\zeta}(t) \neq \boldsymbol{0}$ since $\boldsymbol{M}_m > \boldsymbol{0}$ and $\boldsymbol{F}_2 > \boldsymbol{0}$. In addition, $V_2(\boldsymbol{e}(t),\boldsymbol{\zeta}(t))$ is radially unbounded. By taking time derivative along the trajectory of (23) and considering the relation (22), $\dot{V}_2(\boldsymbol{e}(t),\boldsymbol{\zeta}(t))$ can be calculated as

$$\begin{aligned} \dot{V}_2(\boldsymbol{e}(t),\boldsymbol{\zeta}(t)) &= \frac{1}{2}(-(\boldsymbol{K}_m(p(t),q(t),r(t)) + \boldsymbol{F}_1)\boldsymbol{\zeta}(t) \\ &\quad -\boldsymbol{T}^T(\psi(t))\boldsymbol{F}_2\boldsymbol{e}(t))^T\boldsymbol{\zeta}(t) \\ &\quad +\frac{1}{2}\boldsymbol{\zeta}^T(t)(-(\boldsymbol{K}_m(p(t),q(t),r(t)) + \boldsymbol{F}_1)\boldsymbol{\zeta}(t) \\ &\quad -\boldsymbol{T}^T(\psi(t))\boldsymbol{F}_2\boldsymbol{e}(t)) \\ &\quad +\frac{1}{2}\dot{\boldsymbol{e}}^T(t)\boldsymbol{F}_2\boldsymbol{e}(t) + \frac{1}{2}\boldsymbol{e}^T(t)\boldsymbol{F}_2\dot{\boldsymbol{e}}(t) \\ &= -\boldsymbol{\zeta}^T(t)(\boldsymbol{K}_m(p(t),q(t),r(t)) + \boldsymbol{F}_1)\boldsymbol{\zeta}(t) \\ &= -\boldsymbol{\zeta}^T(t)\boldsymbol{F}_1\boldsymbol{\zeta}(t). \end{aligned} \tag{25}$$

It should be noted that $V_2(\boldsymbol{e}(t),\boldsymbol{\zeta}(t))$ is a continuously differentiable, radially unbounded, positive definite function. $\dot{V}_2(\boldsymbol{e}(t),\boldsymbol{\zeta}(t))$ is always non-positive for any $\boldsymbol{\zeta}(t)$ since $\boldsymbol{K}_m(p(t),q(t),r(t))$ is a skew symmetric matrix and $\boldsymbol{F}_1 > \boldsymbol{0}$. Note that $-\boldsymbol{\zeta}^T(t)\boldsymbol{K}(p(t),q(t),r(t))\boldsymbol{\zeta}(t) = 0$. Let $S_2 = \{(\boldsymbol{e}(t),\boldsymbol{\zeta}(t)) \mid \dot{V}_2(\boldsymbol{e}(t),\boldsymbol{\zeta}(t)) = 0\}$. Then, it is clear that no solution can stay identically in S_2, other than the trivial solution $\boldsymbol{e}(t) = \boldsymbol{0}$ and $\boldsymbol{\zeta}(t) = \boldsymbol{0}$. Hence, from Krasovskii-LaSalle's principle, the origin of (23) is globally asymptotically stable. Thus, the control system can be stabilized by the controller.

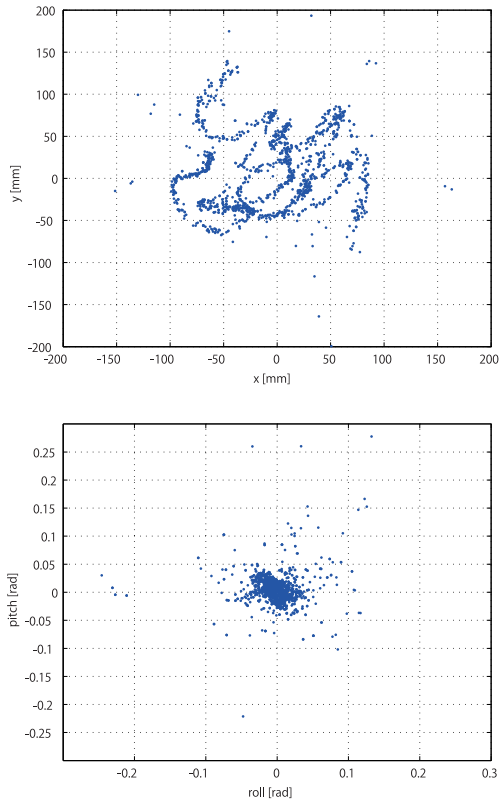

Fig. 3. Hovering control result without stabilizer (x-y and roll-pitch plots).

V. Flight Experiments

Section V shows flight control results without/with the PAS. To simply verify the effect of the PAS during feedback control, we first consider the hovering situation. Next, we carry out flight tasks to desired waypoints.

Fig.3 shows the hovering control result (on the x-y plane and the roll-pitch plane) without the stabilizer, where the target positions of x and y are 0 [mm] and 0[mm], respectively. The control result is directly influenced by the low precision vision sensing. In fact, only 47% samples during the control are stabilized in the stable region Ω, where Ω is defined as $\Omega = \{(\phi(t),\theta(t)) | \sqrt{\phi^2(t) + \theta^2(t)} < 0.05\}$. $\phi(t)$ and $\theta(t)$ denote the roll and pitch angles, respectively. Thus, it is difficult to stabilize the helicopter only using a single vision sensor in real world environment. Fig.4 presents the hovering control result with the PAS. All 100% samples during the control are stabilized in the stable region Ω. The experiment results demonstrate that the PAS renders stable flight in real world environment.

Next, we carry out a flight task for a rectangular trajectory formed by four desired waypoints from (x(0), y(0)) =(0[mm], 0[mm]) at keeping z(t)=1000 [mm]. The vertex points of the rectangular trajectory are Point A (0 [mm], 0 [mm]), Point B (2000 [mm], 0 [mm]), Point C (2000 [mm], 1500 [mm]) and Point D (0 [mm], 1500 [mm]). Figs. 5 and 6 show the

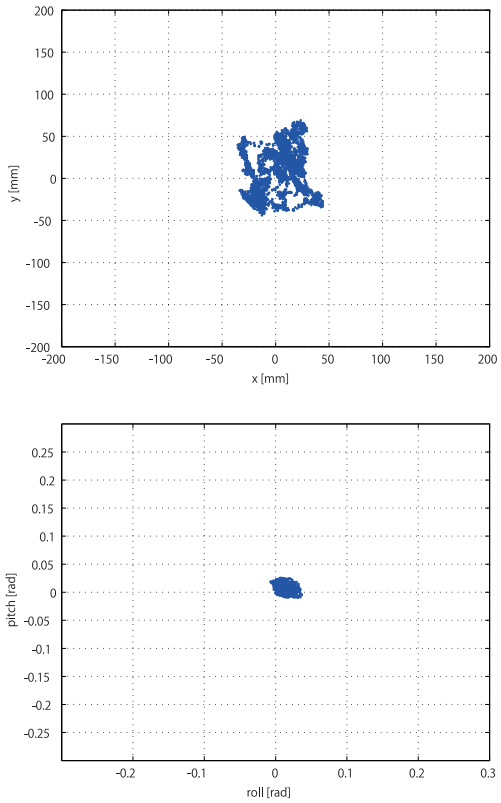

Fig. 4. Hovering control result with stabilizer (x-y and roll-pitch plots).

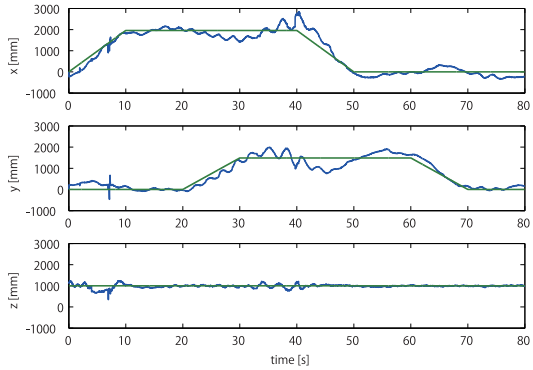

Fig. 5. Waypoint flying control result (without stabilizer).

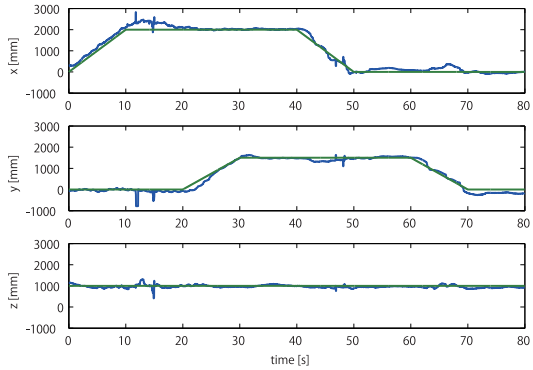

Fig. 6. Waypoint flying control result (with stabilizer).

trajectory control results (x, y and z) without/with the PAS, respectively, where the green and blue lines denote the targets and control results, respectively. It can be seen that the control with the PAS achieves more stable flight. Fig. 7 shows the roll and pitch angles plot without/with the PAS, respectively. 19% samples and 86% samples during the A, B, C and D waypoint hoverings are stabilized in Ω, respectively. In addition, the maximum roll and pitch amplitudes in the stabilizer-case are much smaller than those in the non-stabilizer case. Fig. 8 also shows the trajectory control result with the PAS. The difference between Fig. 8 and Fig. 6 is that the flight in Fig. 8 is required to fly two times faster than that in Fig. 6. Even in this case, the control system is still stabilized, although the non-stabilizer case cannot keep the altitude as soon as control starts. In particular, the roll and pitch angles rapidly increase due to no effect of passive stabilizer.

A drawback of using the gasbag is that it might restrict the motion of the helicopter. However, the experimental results show the utility of the PAS proposed in this paper. Thus, our framework gives a possible solution for visual information gathering tasks (via the palm-size helicopter) from the air in indoor environments. Larger h and r_a realize faster convergence. Conversely, smaller r_a miniaturizes the size of gasbag. Thus we can design h and r_a by considering the balance among its motion restriction, the size of gasbag and the degree of stability. The optimum design for h and r_a depends on considered tasks in given indoor environments and will be one of our future subjects.

Table III shows a comparison with the existing palm-size aerial vehicle control studies [1], [2], [3], [4]. As mentioned before, our eventual research objective is to realize visual information gathering tasks in narrow indoor spaces. Hence, in Table III, small aerial vehicles whose widths are less than 40 [cm] are presented. Excepting our work, the existing small aerial vehicle control studies are achieved with external sensors or external markers. This situation means that the small aerial vehicles cannot be controlled outside external sensor/marker areas. In other words, they showed only hovering results since the small aerial vehicles cannot widely flight outside external sensor/marker areas. The class (less than 40 [cm] width) of small aerial vehicles currently needs assistance of the passive stabilizer in order to widely flight by automatic control in narrow indoor spaces. The work [4] has dealt with two kinds of small aerial vehicles. One of them is extremely small (13.6 [cm]). If the passive stabilizer can be installed to the extremely small helicopter, it may be able to widely flight. Thus, if a much smaller size helicopter is developed, the gasbag size itself can be relatively miniaturized and our framework can be still applied to a much smaller helicopter with a smaller gasbag. In fact, since automatic control of a much smaller helicopter becomes more difficult, the passive stabilizer is useful in practice and a much smaller helicopter with a smaller gasbag can be applied to visual information gathering tasks in much narrower space environments.

TABLE III

COMPARISON WITH THE EXISTING PALM-SIZE AERIAL VEHICLE CONTROL STUDIES.

	Weight [g]	Size [cm] (incl. rotors)	Sensors	Markers	Control	Stability Analysis
Our work	235	35	Camera (internal)	None	Hovering, Trajectory	Done
Yoshihata [1]	220	35	Two cameras (external)	4 markers	Hovering	None
Wu [2]	230	36	Camera (external)	6 markers	Hovering	None
Kubota [3]	255	35	Camera (internal)	Line marker (on field)	Hovering	None
Wang [4]	12.3	13.6	Pan-tilt camera (external)	Marker	Hovering	Done (linear)
	195	36	Pan-tilt camera (external)	Marker	Hovering	Done (linear)

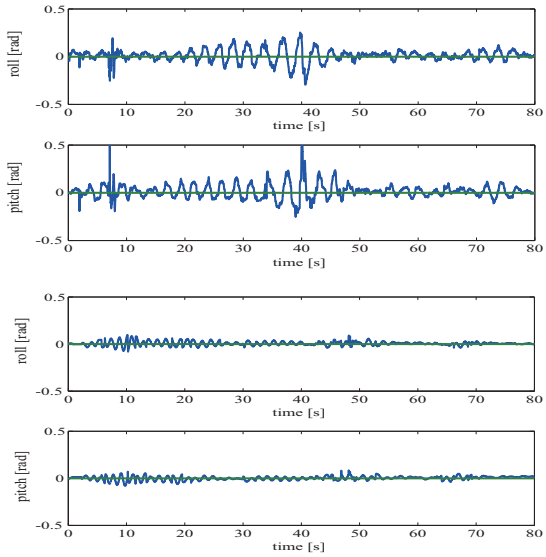

Fig. 7. Roll and pitch plot (Upper two plots:without stabilizer, Lower two plots:with stabilizer.)

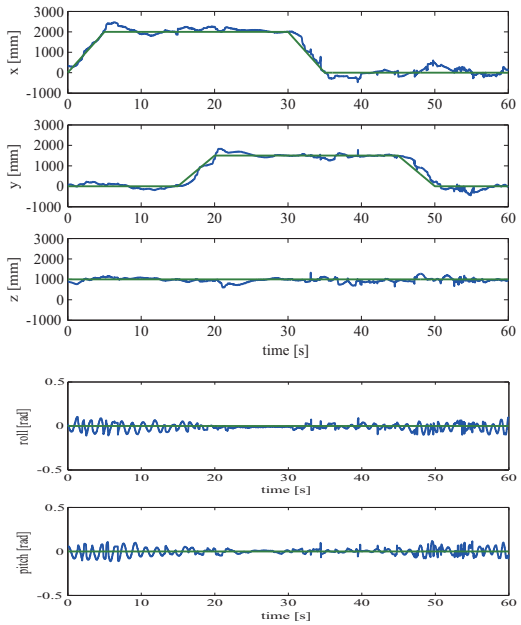

Fig. 8. Waypoint flying control result with stabilizer (faster movement).

VI. CONCLUSIONS

This paper has presented a simple PAS for vision-based stabilization of palm-size aerial vehicles. First, a mathematical dynamic model of a palm-size aerial vehicle with the PAS proposed in this paper has been constructed. Stability analysis for the dynamics has been carried out in terms of Lyapunov stability theory. The analysis results have shown that the proposed stabilizer guarantees passive stabilizing behavior, i.e., passive attitude recovering, of the aerial vehicle for small perturbations from a stability theory point of view. Experimental results have demonstrated the utility of the proposed PAS for the aerial vehicle.

REFERENCES

[1] Y. Yoshihata, et al., Multi-camera visual servoing of a micro helicopter under occlusions, 2007 IEEE/RSJ International Conference on Intelligent Robots and Systems, pp.2615-2620 San Diego, CA, USA, Oct., 2007.

[2] S. Wu, et al., "Indoor autonomous hovering control for a small unmanned coaxial helicopter," 8th IEEE International Conference on Control and Automation, Xiamen, June 2010, pp.267-272.

[3] Y. Kubota, et al., "Dependable visual servo control of a small-scale helicopter with a wireless camera," 15th International Conference on Advanced Robotics, Tallinn, June 2012, pp.476-481.

[4] W. Wang, et al.:Autonomous Control for Micro-Flying Robot and Small Wireless Helicopter X.R.B, 2006 IEEE/RSJ International Conference on Intelligent Robots and Systems, pp.2906-2911, Beijing, Oct., 2006.

[5] P. Freeman, et al., Model-Based and Data-Driven Fault Detection Performance for a Small UAV, IEEE/ASME Transactions on Mechatronics, Vol.18, No.4, pp.1300-1309, August 2013.

[6] M. S. Huq, et al., Magnetic Characterization of Actuators for an Unmanned Aerial Vehicle, IEEE/ASME Transactions on Mechatronics, 2014 (IEEE Early Access Articles).

[7] K. Tanaka, et al., Development of a Cyclogyro-Based Flying Robot With Variable Attack Angle Mechanisms, IEEE/ASME Transactions on Mechatronics Vol.12,No.5, pp. 565-570, 2007

[8] W. Khan and M. Nahon, Toward an Accurate Physics-Based UAV Thruster Model, IEEE/ASME Transactions on Mechatronics, Vol.18, No.4, pp.1269-1279, August 2013.

[9] S. H. McIntosh, et al., Design of a mechanism for biaxial rotation of a wing for a hovering vehicle, IEEE/ASME Transactions on Mechatronics, Vol.11, No.2, pp.145-153 2006.

[10] M. Barczyk and A. F. Lynch, Control-Oriented Modeling of a Helicopter UAV with a Bell-Hiller Stabilizer Mechanism, 2013 American Control Conference, pp.313-320, Washington DC, USA, June, 2013.

[11] Proxflyer, "Picoflyer description," http://www.proxflyer.com/pi_meny.htm, March 2014.

[12] G. Klein and D. Murray, "Parallel Tracking and Mapping for Small AR Workspaces," Proc. of the 6th IEEE and ACM International Symposium on Mixed and Augmented Reality, Nara, Nov. 2007, pp.225-234.

[13] H. Zhang and J. P. Ostrowski, "Visual servoing with dynamics: Control of an unmanned blimp," in Proc. IEEE Int. Conf. Robot. Autom., May 1999, pp. 618-623.

[14] F. Iida, "Biologically inspired visual odometer for navigation of a flying robot," Robot. Auton. Syst., vol. 44, no. 3/4, pp. 201-208, 2003.

[15] B. Etkin, L. D. Reid, Dynamics of Flight, Stability and Control, McGraw-Hill, Third Edition, 1996.

[16] H. K. Khalil, Nonlinear systems, Third Edition, Prentice Hall,2002.